BIOCHEMISTRY
including biophysical chemistry & molecular biology
Article

Biochemistry **2010,** *49,* 9161–9170 9161
DOI: 10.1021/bi1011578

Correlation of Charge, Hydrophobicity, and Structure with Antimicrobial Activity of S1 and MIRIAM Peptides†

Sebastian Leptihn,[‡,⊥] Jia Yi Har,[‡,#] Thorsten Wohland,*[,‡,§] and Jeak Ling Ding*[,‡,∥]

[‡]*Singapore-MIT Alliance, Singapore 117576,* [§]*Department of Chemistry, and* [∥]*Department of Biological Sciences, National University of Singapore, Singapore 117543* [⊥]*Present address: Chemistry Research Laboratory, Oxford University, 12 Mansfield Road, Oxford OX1 3T, U.K* [#]*Present address: Civil and Environmental Engineering, Massachusetts Institute of Technology, 77 Massachusetts Ave., MIT 48-331, Cambridge, MA 02139.*

Received July 21, 2010; Revised Manuscript Received September 23, 2010

ABSTRACT: Antimicrobial peptides are key elements of the innate immune system. Many of them interact with membranes of bacteria leading to perturbation of the lipid bilayer and eventually to inactivation of the pathogen. The emergence of multidrug-resistant bacteria has necessitated innovations of new and more powerful classes of antimicrobials. Here we present the in-depth study of an antimicrobial peptide, MIRIAM, derived from Sushi1 (S1), a well-characterized peptide from the horseshoe crab. MIRIAM interacts strongly with negatively charged lipids, forming an α-helical structure. MIRIAM was found to neutralize LPS and kill Gram-negative bacteria with high efficiency, while not releasing LPS. The promising therapeutic potential of MIRIAM is shown by hemolytic assays, which demonstrate that eukaryotic membranes are unaffected at bactericidal concentrations. Nanoparticle-conjugated MIRIAM used in single-molecule fluorescence and electron microscopy experiments showed that MIRIAM targets bacterial membranes to kill bacteria similarly to parental S1. Furthermore, fragments derived from MIRIAM and S1 provided insights on their molecular mechanisms of action, in particular, the relationships of functional motifs comprised by charge, hydrophobicity, and structure within each peptide. We conclude that the combination of charge, hydrophobicity, and length of the peptide is important. A close interaction of amino acids in a single molecule in a carefully balanced ensemble of sequence position and secondary structure is crucial.

The innate immune system of multicellular organisms employs antimicrobial peptides (AMPs) as the first line of defense to respond quickly and adequately to the invasion of pathogens (*1*). As key elements of the innate immune system, AMPs target a wide range of pathogens, including Gram-positive bacteria, Gram-negative bacteria (GNB), fungi, and protozoa (*2*, *3*). AMPs also play a central role in recruiting and promoting elements of the innate immune system of most living organisms (*4*, *5*).

With an increasing number of multidrug-resistant bacteria, there is a need to develop new and more potent classes of antibiotics (*6*). Therefore, AMPs are valuable alternatives to classical antibiotics, especially cationic AMPs which have many desirable features of a novel antibiotic class. In particular, many AMPs have a broad spectrum of activity: kill bacteria rapidly, are unaffected by classical antibiotic resistance mutations, neutralize LPS, and are active in animal models. As antimicrobial peptides target the membrane structure, pathogens can only acquire resistance by a fundamental change in membrane composition. Hence, the evolution of pathogen resistance to AMPs may be a slow process. In addition to the net positive charge, many cationic AMPs share similar features of hydrophobic and hydrophilic amino acid residues arranged in an amphipathic α-helix (*1*, *7*). However, the diversity in structure and sequence of AMPs complicates the search for common features required for selective antimicrobial activity (*7*). AMP selectivity seems to stem from their charge and resulting electrostatic interactions whereas hydrophobicity is apparently more important for membrane interaction (*8*). However, the situation is far more complicated since other structural parameters such as the position of charged residues and relative size of hydrophobic and hydrophilic cores are believed to influence peptide−membrane interaction (*9*). Also, thermodynamic studies or high-throughput screening for AMPs has shown that there are further crucial properties of the peptides which may be exploited to maximize their interaction with membranes, such as salt bridge formation or "imperfectly amphipathic" structure with either one charged residue or two polar residues within the otherwise hydrophobic core (*10*−*17*). Many studies examined AMPs and compared them to derivatives where the net positive charge and hydrophobicity were altered (*11*−*16*, *18*−*24*). However, the modification of a peptide by a single amino acid residue generally results in the change of more than one parameter, e.g., helicity or amphipathicity.

Sushi 1 (S1)[1] is an extensively studied antimicrobial peptide of 34 amino acid length and is derived from the factor C protein of the horseshoe crab (reviewed in ref *10*). S1 assumes an amphipathic

†This work was supported by the SMA II program, Ministry of Education grant (T208B3109), and a grant by the Faculty Research Committee of the National University of Singapore (R -143-000-338-112).

*Corresponding authors. T.W.: tel, (65)-6516-1248; fax, (65)-6779-1691; e-mail, chmwt@nus.edu.sg. J.L.D.: tel, (65)-6516-2776; fax, (65)-6779-2486; e-mail, dbsdjl@nus.edu.sg.

[1]Abbreviations: DTT, dithiothreitol; POPC, 1-palmitoyl-2-oleoyl-*sn*-glycero-3-phosphocholine; POPE, 1-palmitoyl-2-oleoyl-*sn*-glycero-3-phosphoethanolamine; POPG, 1-palmitoyl-2-oleoyl-*sn*-glycero-3-phospho-(1'-*rac*-glycerol); POPS, 1-palmitoyl-2-oleoyl-*sn*-glycero-3-phospho-L-serine (sodium salt); LPS, lipopolysaccharide; QDot, semiconductor quantum dot; SDS, sodium dodecyl sulfate; S1, Sushi 1 antimicrobial peptide; TFE, trifluoroethanol.

Published on Web 09/28/2010

α-helical structure and carries a net positive charge of +4 at physiological pH. S1 not only possesses antibacterial properties against GNB but also binds and neutralizes LPS from the bacterial cell wall. As hydrophobicity, charge, amphipathicity, and structure are all interdependent on each other, we posed several key questions: What were the characteristic features that render S1 a bactericidal and selective peptide? Would a designed peptide using only the molecular building blocks from S1 be active? If so, would it have the same mechanism of action? What defined the antimicrobial activity exactly? To answer these questions, we rearranged the entire S1 peptide sequence and created an amphipathic helix, which completely changed the sequence but maintained the overall charge and composition of amino acids. Henceforth, this new analogue is referred as MIRIAM. Furthermore, we fragmented both the parental S1 and MIRIAM into their functional moieties predicted *in silico* (Supporting Information Table 1) and compared them with the full-length peptides in their biological and biophysical properties. By using various real time biophysical approaches as was previously employed in our studies with S1 (*8*), we were able to confirm that an association event occurred in which these peptides formed clusters of high concentration in order to exert their function on the GNB membrane, which is consistent with the action of S1. AMPs have been compared with derivatized peptides to determine which factors of a peptide are responsible for its activity and selectivity toward microbial membranes. The aim of this work was to gain deeper insights into the mechanisms of action of the AMPs at a molecular level, albeit not by changing parameters such as charge or hydrophobicity which has revealed essential information for the understanding of AMPs in the past (*11*, *21*, *23*−*26*). In this study, we kept the amino acid composition constant and therefore preserved the overall physicochemical parameters but altered sequence and structure. Toward the goal of understanding the mechanism of action of the new and its parental AMP, the fragmentation of the peptides proved to be very useful in revealing the relationships of charge, hydrophobicity, or amphipathicity and structural patterns within an AMP.

MATERIALS AND METHODS

Peptides. Peptides were synthesized by Genemed Synthesis Corp. (San Francisco, CA, USA). MIRIAM has the following sequence: MIRIAMKALNCFKVSGLKCWSFNSPRGQESPCPG. Fragments of MIRIAM were MIRIAMKALNCF (MIR-F1) and KVSGLKCWSFNSPRGQESPCPG (MIR-F2). Sushi 1 peptide has the sequence GFKLKGMARISCLPNGQWSNFPPKCIRECAMVSS. Fragments S1-F1 and S1-F2 have the sequences GFKLKGMARI and SCLPNGQWSNFPPKCIRECAMVSS, respectively. A Sushi 1 mutant named negS1 was used as negative control; the first three lysine (K) and arginine (R) residues were changed to glutamate (E) (GFELEGMAEISCLPNGQWSNFPPKCIRECAMVSS). All peptides were synthesized as N-terminally unmodified as well as biotinylated.

Fluorescence Spectroscopy. Fluorescence emission spectra were recorded on a spectrofluorometer (Model LS 50B; Perkin-Elmer, Canada). Measurements were performed between 300 and 450 nm at 1 nm increments using a 5 mm quartz cell at room temperature. The excitation wavelength was set to 280 nm with both the excitation and emission slit width set to 4 nm. Spectra were baseline-corrected by subtracting blank spectra of the corresponding lipid or detergent solutions without the peptide. The samples contained 2 μM peptide and 0.5 mM lipid or 10 mM detergent. Measurements were performed in phosphate-buffered saline (PBS, pH 7.4).

Circular Dichroism Measurements. Spectra were obtained using a spectropolarimeter (Model Jasco-J-810; Jasco, Easton, MD, USA). Each spectrum was recorded from 190 to 260 nm as an average of six scans using a quartz cuvette with a 1 mm path length at room temperature. The scanning speed was 30 nm/min at a step size of 1 nm, a 2 s response time, and a 1 nm bandwidth. All peptide samples were at 50 μm in PBS, pH 7.4. The concentration of POPG/POPE (3:1) or POPC was 2 mM, whereas the concentration of LPS was 400 μg/mL. Spectra were corrected by subtracting the corresponding spectra from samples containing no peptide. Raw data were used to calculate Theta residues; the program CDNN was used to calculate the percentage of secondary structural features.

LPS Neutralizing Assay (*rFC Assay*). The LPS neutralization was quantified using a PyroGene kit (Lonza Inc., USA) according to the manufacturer's instructions. The principle of this assay is the activation of recombinant factor C (rFC) by LPS. Upon activation the enzyme hydrolyses a fluorogenic substrate which emits light at 440 nm (with an excitation wavelength of 380 nm). Measurements were performed on a plate-reader spectrofluorometer (Model: LS 50B; Perkin-Elmer, Canada). The samples are measured every 3 min. Positive (LPS in PBS, pH 7.4) and negative (PBS, pH 7.4 only) controls were included in each run. From triplicate measurements, the mean values with standard error and standard deviation were obtained as a function of time.

Surface Plasmon Resonance (*SPR*). The interactions between the peptides and phospholipids on the solid-phase substrate were studied by SPR, where lipid A from *Escherichia coli* strain O55:B5 (Sigma-Aldrich, Singapore) was coated on an HPA chip to mimic the biological membrane. The real-time interaction between different concentrations of peptides and phospholipids in PBS (pH 7.4) was performed using a Biacore 2000 (GE Healthcare, Singapore). The SPR was recorded on the phospholipid-coated HPA chip. The HPA chip was regenerated by a pulse of 0.1 N NaOH until the SPR reached baseline. The response units (RU) were baseline-corrected by subtraction of RU from a blank solution without peptide. The temperature within the sample chamber was maintained at 25 °C.

Antimicrobial Assay. To test the bacteriostatic or bactericidal ability of the peptides, the BacTiter-Glo microbial cell viability assay (Promega, USA) was performed according to the manufacturer's instructions using dilutions of *E. coli* ATCC 25922. The bacteria were washed in PBS (pH 7.4) and resuspended in PBS (pH 7.4) containing 2 μM peptides and then incubated at 37 °C. Survival was monitored by determination of the cellular ATP content using BacTiter-Glo microbial cell viability assay (Promega, USA) using a luminometer (Glomax 20/20; Promega, USA).

Hemolytic Assay. The hemolysis assay was adapted from the method of Shin et al. (*27*). Rabbit erythrocytes were used to test the hemolytic activities of the peptides. Whole blood was collected in a sterile, heparinized, borosilicate tube and centrifuged (3K10 centrifuge; Sigma) at 1000*g* for 5 min at 4 °C. The supernatant, including the leukocytes above the erythrocyte pellet, was removed carefully and discarded. Intact erythrocytes were washed three times with 3 volumes of prechilled PBS (pH 7.4). Erythrocyte suspensions were adjusted to 0.8% for the hemolysis assay. Dilutions of the peptides were prepared in PBS (pH 7.4), and equal volumes of 0.8% erythrocyte suspension were mixed with peptide solutions in sterile disposable plastic tubes. The tubes were incubated at 37 °C. After 1 h intact cells were

sedimented by centrifugation, and the amount of hemoglobin released into the supernatant was determined by reading the absorbance at 414 nm against a reference wavelength of 490 nm. A positive control of 0.4% erythrocyte lysed in 10% SDS was taken as 100% lysis. The negative control was erythrocytes in PBS (pH 7.4) alone, which gave minimal lysis. This was taken as 0%.

Fluorescence Microscopy. Measurements were performed as described before (*8*). A fluorescence microscope (Axiovert 200M; Carl Zeiss, Germany) was used to examine the staining of peptide quantum dot (PEG-Qdot; Invitrogen, Singapore) bioconjugates. As labels QDots of the emission wavelengths 525 and 655 nm were used (Invitrogen, USA). The bacteria were attached to poly(L-lysine)-treated glass slides. After addition of the bioconjugates to the samples the glass slides were washed with 1 mL of PBS (pH 7.4).

Transmission Electron Microscopy. *E. coli* ATCC 25922 was grown overnight at 37 °C in Mueller−Hinton broth; 1×10^9 cells/mL were washed three times with phosphate-buffered saline (PBS, pH 7.4) and resuspended in the original volume in PBS. Nanogold particles of 10 nm size (Sigma-Aldrich, Singapore) were covalently linked to streptavidin (Invitrogen, Singapore) and then conjugated with a 1:1 ratio of N-terminal biotinylated MIRIAM. Nonbiotinylated MIRIAM was added to a ratio of 1:5 (nanogold:peptide). One hundred microliters of this solution was mixed with 100 μL of *E. coli* (final concentration 1 μM). After 30 min the bacteria were washed twice with 1 mL of PBS (pH 7.4) each and fixed by the addition of 2.5% glutaraldehyde and 2% paraformaldehyde, which cross-link proteins and peptides and trap carbohydrates, lipids, and nucleic acids in the bacterium. Following that a 12 h lipid fixation with 1% osmium tetroxide in PBS was performed. Subsequently, a standard TEM sample protocol was followed with dehydration steps before embedding in resin as described previously (*8*). After microtomy and transfer of the sample preparations onto Formvar copper grids, the samples were stained by uranyl actetate (10%, 10 min) and lead citrate (1.5%, 5 min). As controls, negS1 or biotin was used together with the nanogold particles. In addition, nanogold with nonbiotinylated MIRIAM was used. The samples were observed with a Philips CM10 TEM using a primary magnification of 42000−145000. The nanogold particles were counted to evaluate their distribution on/in the cell.

Fluorescence-Activated Cell Sorting (*FACS*). *E. coli* ATCC 25922 was grown overnight at 37 °C in Mueller−Hinton broth; 1×10^8 cells/mL were washed three times with PBS (pH 7.4) and resuspended in the original volume in PBS. The cells were labeled with peptide-Qdot655 conjugates as described previously (*8*). The FACS analyses of the peptide-Qdot conjugate labeled cells were performed using an Excalibur flow cytometry instrument (excitation 488 nm, emission 675 nm; BD Biosciences). For the experiments, the fluorescence from the MIRIAM-Qdot655 conjugate was compared with the background fluorescence obtained from unlabeled cells as well as *E. coli* labeled with S1-Qdot655 as a positive control.

Fluorescence Correlation Spectroscopy (*FCS*). The FCS system was built around a FV300 Olympus laser scanning confocal microscope, where an additional FCS module was coupled to the microscope. Measurements were performed as described previously (*8*).

Total Internal Reflection Microscopy (*TIRF*)*−Single Particle Tracking* (*SPT*). SPT was performed on a modified EMCCD camera (Cascade 512B; Photometrics) coupled inverted epifluorescence microscope (Axiovert 200 M; Carl Zeiss) in total internal reflection fluorescence mode. Laser light from a 532 nm diode-pumped solid-state laser (Calypso, Cobolt; PhotoniTech) at 5−6 mW was used for excitation, and the emission filter used 645AF75. Measurements were performed as described previously (*8*).

Lipids were purchased from Avanti Polar Lipids (Germany). All other chemicals were purchased from Sigma-Aldrich (Singapore).

RESULTS

Design of a Sushi1-Derived Peptide. For the construction of a new peptide, we used the same amino acid composition and length of S1 and therefore kept the overall charge and polarity constant. The entire peptide sequence was rearranged; then an α-helical peptide was generated at the N-terminus whereby the charge and polarity were distributed resulting in an amphipathic helix. The peptide was designated as MIRIAM due to its first six amino acids. One of the three proline residues was placed in position 26 to create a kink in a region which potentially forms a helix and to end the helix at this point. The other two proline residues were placed in positions 30 and 32. Structure prediction using the GOR V algorithm (*28*) gave an α-helix from residues 1 to 12 followed by a random coil structure from positions 13 to 34. Accordingly, two fragments were synthesized dividing the peptide in two uneven halves, designated MIR-F1 (residues 1−12) and MIR-F2 (residues 13−34) (Figure 1). MIR-F1 contains the α-helical segment supposedly forming an amphipathic helix, whereas the MIR-F2 fragment contains the rest of the amino acid chain of the peptide including the single tryptophan residue. For comparison, we used full-length S1 and S1 fragments (S1-F1 which spans from 1 to 10 and S1-F2 which covers 11−34 amino acids). As a negative control, the peptide negS1 was designed identical to S1 except for the replacement of cationic amino acids for anionic ones. Supporting Information Table 1 provides sequences of the peptides as well as calculated parameters and observed properties.

MIRIAM Interacts with Anionic Phospholipids Undergoing α-Helical Transition. To determine the binding affinity of MIRIAM to negatively charged lipids, we employed surface plasmon resonance (SPR) analysis where POPG or lipid A was immobilized. Measurements to determine binding constants of the peptides to POPG or lipid A showed that MIRIAM has higher affinity than S1 (Figure 2A) for these phospholipids. The dissociation constant of MIRIAM for POPG and lipid A was calculated to be 1.2 nM (± 0.1) and 5.1 nM (±0.1), respectively.

In order to characterize the nature of the interaction between MIRIAM and the lipids, we conducted circular dichroism (CD) spectroscopy. In buffer, the peptide showed no defined secondary structure, as was the case with S1, showing a minimum around 198 nm (Figure 2B, Sushi 1; see Supporting Information Figure 1). In a 40% TFE solution which is known to induce α-helices in peptides (*29*) the full-length MIRIAM peptide adopted an α-helical structure of about 25% according to deconvolution with CDNN. In the presence of the micelle-forming detergent, SDS, as well as the negatively charged lipid POPG/POPE, MIRIAM adopted a partial α-helical structure. Interestingly, the degree of α-helicity was highest when in POPG/POPE, showing the specificity of the peptide for negatively charged lipids. No structural change in MIRIAM was observed when in the presence of a mammalian analogue membrane phospholipid, POPC, a lipid that lacks net negative charge (data not shown).

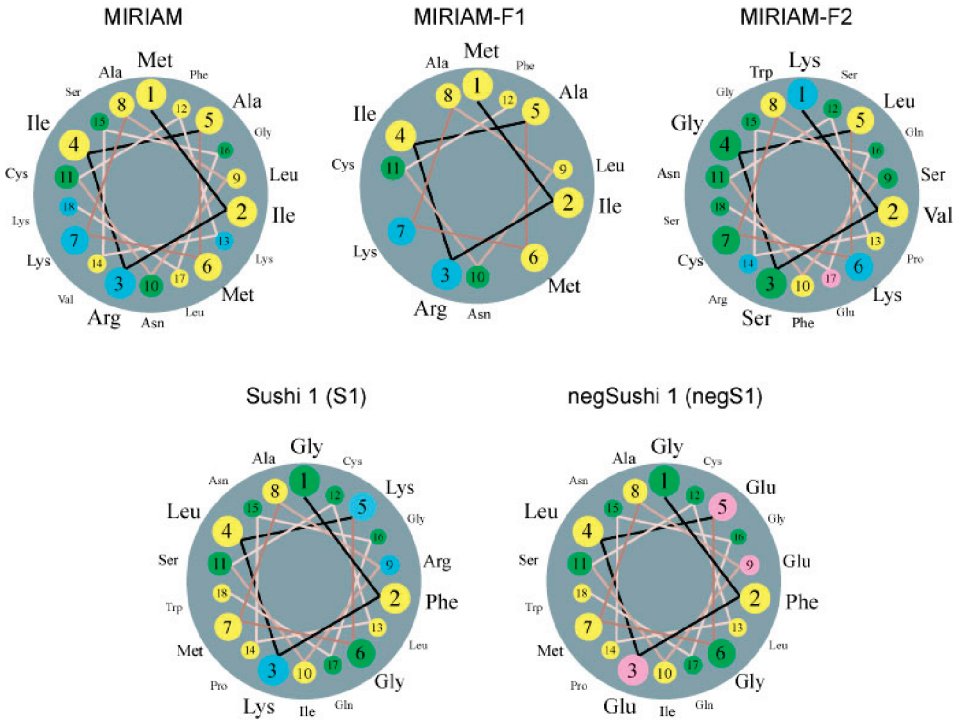

FIGURE 1: Peptides and peptide fragments. Helical wheel projection of the full-length (top) MIRIAM peptide and fragments MIR-F1 (left) and MIR-F2 (right). Helical wheel projections visualize the distribution of hydrophobic (yellow) and polar residues (green) with respect to the helical axis, illustrating the amphipathic structure of MIRIAM and MIR-F1. Basic and acidic residues are displayed in cyan and red, respectively.

From these observations we can conclude that MIRIAM adopts an α-helical structure when interacting with negatively charged lipids but does not interact with zwitterionic lipids.

To further study the nature of interaction of MIRIAM with membranes, we conducted fluorescence spectroscopy using intrinsic tryptophan fluorescence. A different emission peak was observed when exposed in a hydrophilic environment such as buffer, compared to when the aromatic amino acid was in a hydrophobic surrounding such as lipids where the emission was blue shifted. This physical effect was used to determine the insertion of the peptide into lipids (Figure 2C). MIRIAM shows a tryptophan emission peak shift in an anionic lipid containing and SDS environment. Generally, insertion of a tryptophan-containing peptide into a hydrophobic environment results in a blue shift of the emission maximum, together with an increase of the quantum yield (*30*). However, the blue shift for the binding of MIRIAM peptides to POPG/POPE was accompanied by a decrease in the fluorescence intensity, in contrast with the behavior of other peptides (*31*). Possibly the quenching of the tryptophan indole moiety by arginine and lysine side chains in the MIRIAM peptides might account for this effect. It has been shown that the side chains of eight amino acids, including lysine, can quench tryptophan fluorescence (*32*, *33*). Peptide conformational changes accompanying binding of MIRIAM to negatively charged vesicles might decrease the distance between one or more lysines or arginines and the tryptophan and therefore result in fluorescence quenching of the residue.

Since three cysteine residues are found in the peptide, we performed the measurements under reducing conditions (1 mM DTT) as well as under oxidizing conditions (air oxidizing to allow disulfide bridge formation). No spectral shift was observed, indicating no interaction under oxidizing or reducing conditions (data not shown). Taken together, we conclude that MIRIAM inserts into negatively charged lipids, a property which is commonly observed for AMPs of the α-helical group. Similar to the parental peptide, electrostatic interaction seems to be the crucial factor for lipid binding as shown with the zwitterionic lipid, POPC (*8*). Moreover, there was no indication from activity assays that the peptides were forming dimers via disulfide bridges to confer their binding capability.

MIRIAM Neutralizes LPS and Is Highly Effective against GNB While Showing Low Hemolytic Effect. To determine the biological activity of MIRIAM, we tested its ability to neutralize LPS. The *in vitro* assay we used was based on the activity of recombinant factor C (rFC) which is activated by LPS, leading to the cleavage of a fluorogenic substrate. Samples which did not bind and neutralize LPS, such as the control peptide negS1, showed fluorescence similar to internal control reactions only containing LPS. MIRIAM at <0.5 μM concentration efficiently neutralized high amounts of LPS (2 EU/mL) (Figure 3A, Supporting Information Figure 2), with an IC_{50} value of 155 nM (±3.1 nM). This confirms that MIRIAM has similar activity to its parental peptide S1, which, in order to completely suppress rFC activity, needs to be present at more than a 2.5 μM concentration.

To determine the antibacterial potential of MIRIAM, we employed an antimicrobial assay based on ATP quantification in cells using luciferase. Outside cells, ATP is decomposed rapidly, implying that the detected ATP hydrolysis corresponds to ATP in intact cells. *E. coli* washed in PBS (pH 7.4) were quickly killed by MIRIAM, whereas the control shows a decrease solely due to starvation of bacterial cells, resulting from decreased metabolic rate, hence decreased cytosolic ATP. At a concentration of 2 μM MIRIAM the half-time of complete lysis of 3×10^7 bacteria/mL was determined to be 19 min (Figure 3B).

To observe release of LPS from bacteria in the presence of AMPs in real time, we used fluorescence correlation spectroscopy (FCS) of fluorescently labeled LPS molecules in the membrane of

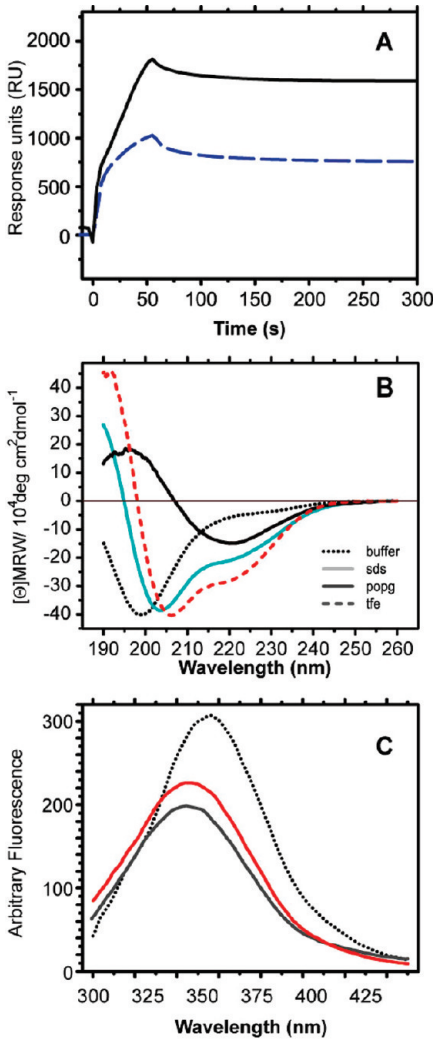

FIGURE 2: Interaction of MIRIAM with lipids. (A) Surface plasmon resonance measurements with MIRIAM (black line) and S1 peptide (dashed blue line) binding to POPG/POPE demonstrate the relative higher affinity of MIRIAM to POPG/POPE. (B) CD spectroscopy of MIRIAM shows that the structure of the peptide changes from random in buffer (black dotted line) to α-helical in POPG/POPE (black solid line), SDS (red dashed line), or TFE (cyan line). (C) The blue shift in tryptophan fluorescence from MIRIAM in buffer (black dotted line) shows that the residue is inserting into vesicles of POPG/POPE (red line) of detergent micelles (SDS, gray line).

E. coli. FCS measures fluorescence intensity fluctuations from a confocal volume and calculates autocorrelation functions which can be fitted with theoretically predetermined models to extract molecular parameters for different fluorescence species (*34*). The number of particles in the focal volume of each species is proportional to their concentration, and thus molar fractions of mixtures can be determined. To determine if MIRIAM disrupts the outer membrane of *E. coli* while releasing LPS molecules from the lipid bilayer, we labeled *E. coli* with the fluorescent dye Alexa Fluor 555 (hydrazine) on the sugar residues of LPS. After incubation with MIRIAM, the cells were pelleted, and the supernatant was analyzed by FCS. Similar to the parental peptide S1, MIRIAM did not cause a release of LPS during lysis in contrast to the mechanism of action of polymyxin B (Figure 3C).

After yielding promising results in the antimicrobial assay, we tested MIRIAM for lysis of eukaryotic cells. As mentioned above, MIRIAM interacts only with negatively charged lipids but does not interact with the zwitterionic POPC. Membranes from eukaryotes differ significantly from microbial membranes in their composition and charge. We used rabbit red blood cells resuspended in PBS. Lysis of the red blood cells would release hemoglobin, which can be detected in the supernatant by measuring the absorbance of hemoglobin. The peptide showed only 3% hemolytic activity at a high concentration of 10 μM (Figure 3D), which is five times higher than the microbicidal concentration. The results illustrate that the peptide is a highly selective AMP with the ability to neutralize LPS and to kill GNB without releasing LPS from the membranes while not disrupting eukaryotic cells.

Fragments of MIRIAM and Sushi1 Interact with Lipids but Lost Their Antimicrobial Activity. In the presence of negatively charged lipids or in solutions of TFE or SDS, the structural properties of MIRIAM fragments differed vastly from each other. In 40% TFE, MIRIAM and MIR-F1 form helical structures, whereas MIR-F2 remained unstructured (Figure 4A). Interestingly, MIRIAM and MIR-F1 consistently formed the highest ordered α-helical structure in POPG/POPE. MIR-F2 again showed no rearrangement of its structure and gave a nonstructured signal in CD analysis (Figure 4B). Even in TFE, $<5\%$ of MIR-F2 may be characterized as α-helical. The acquisition of an α-helical structure of MIRIAM and MIR-F1 in POPG/POPE indicates their interaction with the lipid whereas there is no clear evidence that MIR-F2 interacted with the lipids. The only tryptophan in MIRIAM is found in fragment MIR-F2, which showed no shift in anionic lipids (Figure 4C), indicating that in this fragment the tryptophan residue is not involved in a potential interaction with lipids. However, a decrease in fluorescence intensity of the tryptophan was observed, similar to the full-length peptide. This might indicate a structural rearrangement of the peptide and fluorescence quenching of the tryptophan residue by lysine or arginine induced by the interaction with the lipids (*32*, *33*).

In the case of fragments of S1, the absence of a structural rearrangement shown by CD spectra might indicate that S1-F1 covering amino acids 1−10 does not interact with negatively charged lipids or with TFE (Figure 4D). Similarly, S1-F2 showed a complete random coil with a positive signal at 212 nm for the peptide in buffer or in TFE. However, the peptide transitioned into an α-helical structure in POPG/POPE. To prove or disprove the interpretation that S1-F2 interacts with the lipid, we performed tryptophan fluorescence spectroscopy of the peptide in the presence or absence of POPG/POPE. When in aqueous environment the peptide showed a maximum fluorescence intensity peak at 357.5 nm, which was strongly blue shifted to 349.5 nm when the peptide was preincubated in POPG/POPE-containing solution (Figure 4F). This observation indicates that the peptide S1-F2 interacts with the lipid. Since various blue shifts could be observed in samples that have been incubated for varying periods of time, we followed the shift over time, starting with the addition of the peptide. Interestingly, the insertion of the tryptophan residue was observed to be rather slow, with a half-maximal insertion time of 5947 s (±67 s) (Figure 5). This slow process stands in contrast to the binding of the full-length S1 peptide where the fast insertion could not be measured with the same method due to limited time resolution.

Furthermore, we tested the interaction of the two tryptophan-containing peptide fragments derived from S1 and MIRIAM with the uncharged lipid POPC. As expected, like the parental peptides, neither MIR-F2 nor S1-F2 showed shifts, indicating the

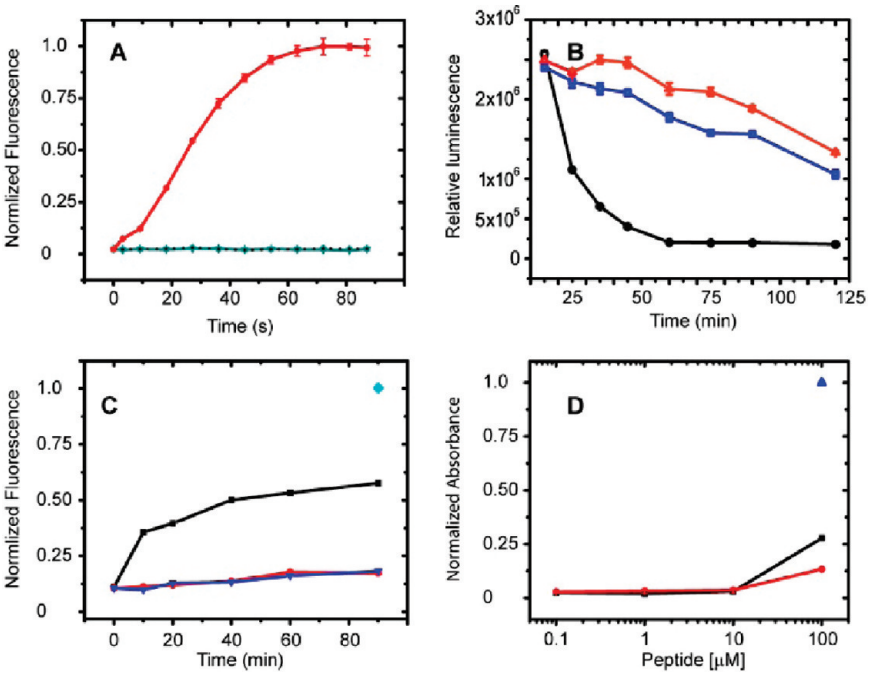

FIGURE 3: Antimicrobial and membrane activity of MIRIAM. (A) LPS neutralization assay shows effective neutralization by MIRIAM (green line) similar to values from samples without LPS (black line). Full activation of rFC is shown in the sample with LPS only (red line). (B) Antimicrobial assay with negS1 (blue line) and MIRIAM (black line). The control without any additive is displayed in red. (C) LPS release assay using FCS. In contrast to PMB (black line), no LPS release can be observed in samples with MIRIAM (red line) or no additive (blue line). 100% LPS release induced by addition of 10% SDS is indicated by a cyan diamond. (D) Hemolytic assay using S1 (red line) and MIRIAM (black line). 100% lysis using 10% SDS is indicated with a blue triangle.

importance of electrostatic interactions between the negatively charged lipid and the positively charged peptides (data not shown). Even though we observed an interaction with negatively charged lipids, neither fragment was able to neutralize LPS on its own or combined with the other half of the respective peptide (MIR-F1 + MIR-F2 or S1-F1 + S1-F2) (Supporting Information Figure 3). Therefore, it is not surprising to observe that both fragments lost bactericidal activity, either combined or on their own in the antimicrobial assay (data not shown).

These results suggest that the full-length MIRIAM peptide is a very potent LPS-neutralizing agent. While fragmentation of MIRIAM abolished its activity, a fragment of the parental peptide S1 was still able to interact with the lipids. It also indicates the importance of the residues flanking either side of the MIR-F1 and MIR-F2 in conferring a full AMP functionality to MIRIAM.

MIRIAM Targets the Outer and Inner Bacterial Membranes but Does Not Enter the Cytosol. We used transmission electron microscopy (TEM) to obtain ultrastructural information regarding where MIRIAM binds to GNB. Nanogold-conjugated MIRIAM at 1 μM was incubated with *E. coli* for 30 min. The conjugate acted differently compared to S1. It detached the GNB membranes but did not enter the cytosol (Figure 6). Membranes stained with osmium tetroxide can be seen separately from the cell, suggesting that MIRIAM binds and, to some extent, even led to the detachment of the membrane of GNB. In contrast to previously published results obtained with S1-nanogold particles, where the peptide conjugates were not only found on the inner and outer leaflet of the inner and outer membranes but also in the periplasmic space and cytosol of the bacterium, the MIRIAM-nanogold particles were only located on detached membranes, appearing grayish (n (cells) = 76). Considering an apparent discrepancy with the SPR data which demonstrated that MIRIAM dissociates from microbial membrane lipids (lipid A and phospholipids), the data obtained here might not be sufficient to conclude that MIRIAM does not dissociate into the cytosol; it emphasizes however, the high-affinity constant of the peptide to the membrane lipids. Controls with nanogold alone confirmed that this result is specific to the peptide functionality. We included negS1-nanogold as well as biotin-nanogold as controls, where no free or bound particles could be observed. A further control included the use of both components separately (nonbiotinylated MIRIAM, biotin-nanogold), not as a peptide-nanogold conjugate. Again, in all controls, particles could not be observed (n = 141). Therefore, it can be concluded that only particles conjugated with MIRIAM were bound to the membranes, demonstrating the specificity of the MIRIAM-nanogold.

These results suggest that MIRIAM acts selectively on the membrane of GNB, similar to the parental peptide S1, but it may not have an internal periplasmic or cytosolic target. It appears that MIRIAM acts by creating major membrane defects, which can lead to the detachment of membranes and therefore to the leakage of cytosolic content, which effectively kills the bacteria.

Fluorescent Nanoparticle MIRIAM-Conjugate Tracking on Live Bacteria Reveals Aggregation of Peptides at Active Concentrations. We used quantum dot labeled MIRIAM in which the conjugates were thoroughly tested for their biofunctional properties as described previously (*8*). MIRIAM-Qdot was used to stain *E. coli*, and the cells were then subjected to flow cytometry (FACS). Binding of the conjugate was efficient (Figure 7A). Interestingly, the binding differed from that of S1-Qdot and showed a broader distribution, with intensely stained bacteria. This might indicate that the bacteria disintegrated as well as aggregated compared to when S1 was applied where the bacteria were homogeneously sized (seen in the distribution of

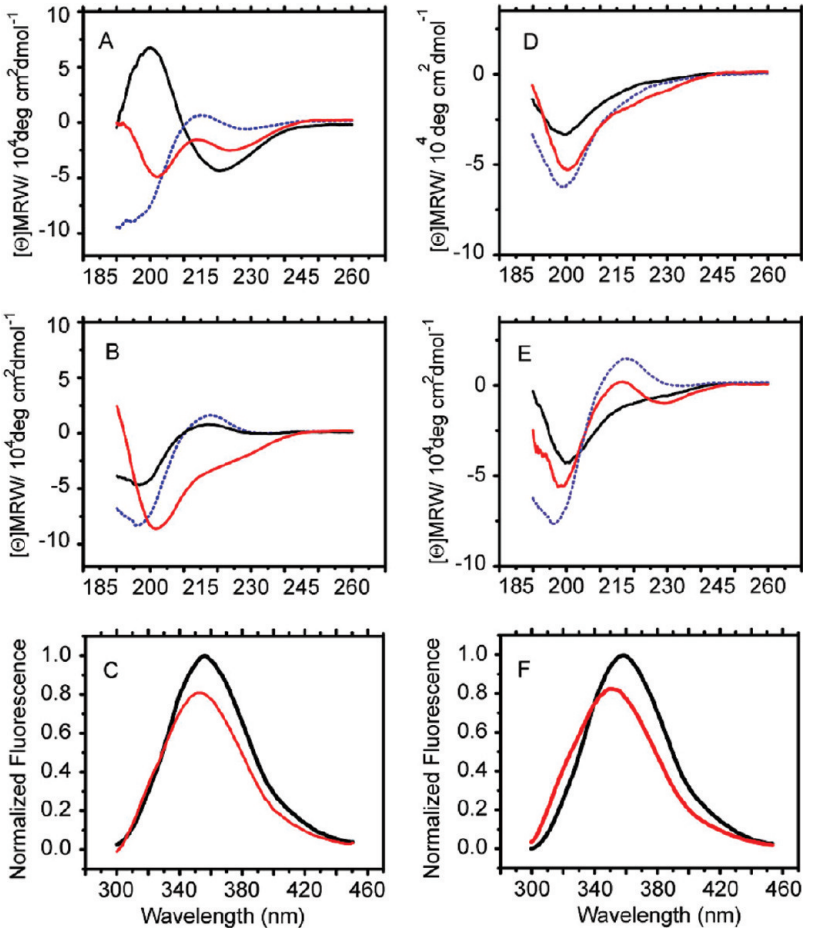

FIGURE 4: Structural characterization of peptide fragments MIR-F1, MIR-F2 and S1-F1, S1-F2. (A) Structural conversion of a random coiled MIR-F1 in buffer (blue dotted line) to an α-helical peptide in TFE (red line) and POPG/POPE (black line). (B) Structural conversion of MIR-F2 from random coil in buffer (blue dotted line) to α-helical structure takes place only in the presence of 40% TFE but not in negatively charged lipid, such as POPG/POPE (black line). (C) No tryptophan-mediated shift of MIR-F2 can be observed in the presence of negatively charged lipid (POPG/POPE, red line) in regard to the emission in buffer (black line). (D) S1-F1 does not change the structure when in buffer (dotted line), in TFE (red) or in POPG/POPE (black line). (E) S1-F2 shows a positive signal at 212 nm typical for random coil in buffer (dotted line) and TFE (red), whereas it changes to a minor content of α-helix in POPG/POPE (black line). (F) The tryptophan in S1-F2 shifts to lower wavelengths in POPG/POPE (red) as compared to buffer (black), indicating insertion into the lipid.

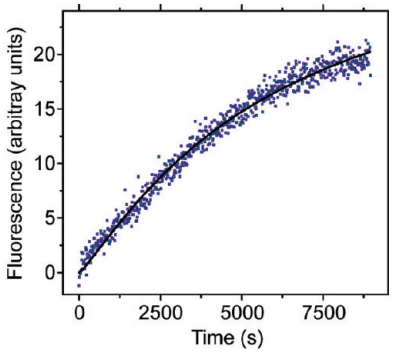

FIGURE 5: Insertion of S1-F2 into POPG/POPE. The half-time of insertion averages to 1.5 h, calculated by fitting the tryptophan emission shift over time with a single-exponential equation. Insertion of the peptide is very slow compared to the parental peptide S1 which inserts faster than this method of measurement allows (> 1 min). Control measurements with peptide only in the absence of lipid showed no change in fluorescence under the same conditions.

sorted cells in the side and forward scatters, Supporting Information Figure 4). Furthermore, the fluorescence spectra of the MIRIAM-Qdot conjugate showed that the previously reported blue shift of the nanoparticle conjugate on *E. coli* was not as prominent, albeit significant compared to S1-Qdot (7 nm compared to 22 nm, Figure 7B). The control negS1-Qdot however showed an emission, which was identical to the emission of the free Qdot measured in aqueous or organic (tetrahydrofuran) solvents (data not shown).

We further employed MIRIAM-Qdots to study the diffusion of the peptides using single particle tracking (SPT) on live bacteria, employing TIRF microscopy. On live *E. coli* cells the average diffusion coefficient (D) of a single MIRIAM-Qdot particle was determined to be 5.52 $\mu m^2/s$ (Figure 7C). The MIRIAM-Qdot conjugates showed a relatively unrestricted lateral movement along the bacterium. The determination of the lateral diffusion coefficient of the conjugates at high concentration of unlabeled peptide (0.5 μM) was reduced to 1.55×10^{-3} $\mu m^2/s$, which is similar to our published measurements of S1-Qdot conjugates. From this we conclude that MIRIAM peptides aggregate on the membrane in order to form membrane-active complexes.

DISCUSSION

To understand the mode of action of a membrane-active peptide on a molecular level, it is essential to study its sequence structure−function relationship. The interactions of the peptides with the membrane are determined by the peptide composition

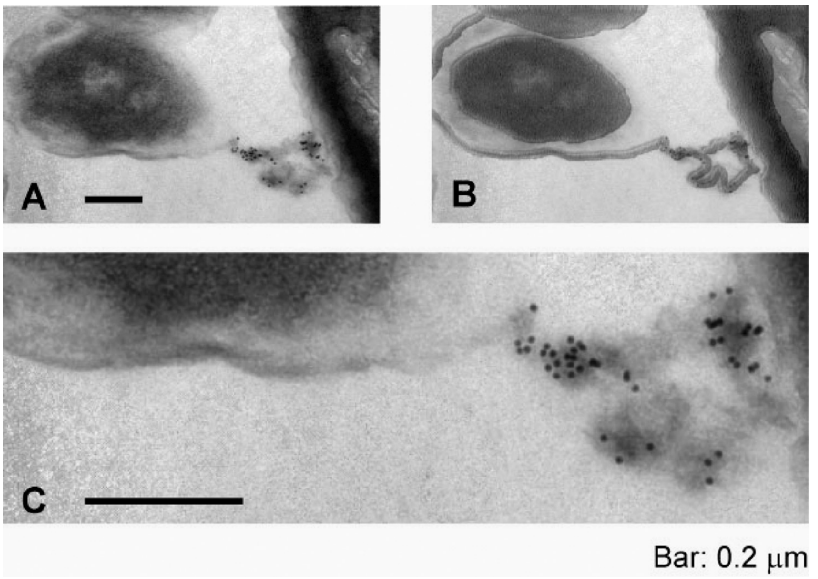

FIGURE 6: TEM of MIRIAM-nanogold conjugates. The particles can only be found attached to the membranes. (A) Representative micrograph showing an *E. coli* cell from which the membranes have been detached by the action of MIRIAM. (B) Illustrative processed version of (A) using ImageJ. (C) Detail of (A) showing the electron dense dark nanogold particle attached to the membrane (gray).

and particular electrostatic properties, but it is not the sequence directly that determines mechanism or specificity per se (*7*). In this work, we analyzed the fundamental basis of this interaction mechanism using a combination of mutagenesis of the naturally occurring sequence of the peptide S1 and exchanges of charge polarity (negS1) as well as a rationally designed peptide using only building blocks of S1 to design a peptide named MIRIAM. In other studies, single amino acids have been replaced with residues of different charge or hydrophobicity. However, this was likely to change the entire peptide and even alter the intramolecular interactions and structure. Our study differed in the main approach where we did not change the overall physicochemical parameters of the parental peptide. Instead, we created a novel peptide by rearrangement of the residues of the S1 sequence in order to create the known amphipathic helical moiety.

The observed selectivity of S1 and MIRIAM for anionic lipids is attributable to electrostatic interactions and correlates well with their antibacterial activities, an observation commonly made with other cationic AMPs (*21*, *26*, *35*). However, the overall charge and hydrophobicity seem not to be the sole factors responsible for antimicrobial activity and cell selectivity (*7*, *11*, *18*, *21*, *23*, *24*, *36*). To better understand the relationship between the structure and activity of MIRIAM and S1, we therefore studied the peptide as shorter fragments. While both the full-length S1 and MIRIAM peptides form α-helices when interacting with anionic lipids, dissection of the peptides into two led to the loss of their antimicrobial activity although some of the fragments still showed a structural change upon interaction with target membranes. Nevertheless, these results suggested that the α-helical structure within an amphipathic helix of the peptides is not the sole determinant of the antibacterial activity (*20*, *24*).

The widely accepted hypothesis states that the initial step of AMP binding to the membrane is mediated by the electrostatic attractions of peptides to the membrane (*7*, *37*). Since both S1 and MIRIAM contain multiple basic amino acid residues, the observed antibacterial activity is likely to stem from the peptide's affinity for negatively charged cell surface components on the outer membrane of GNB. In the case of negS1 in which the cationic amino acids were replaced with anionic amino acids, a clear decrease in affinity for negatively charged lipids, as well as abolishment of antimicrobial functionality, was observed. However, the residual activity of negS1 (such as a low affinity for POPG and *E. coli* membranes and minor antimicrobial activity) indicates that hydrophobicity plays a significant role (*23*). Important information is gained by the study of the C-terminal fragment, S1-F2, which contains positive charges correlating the electrostatic interaction between the full-length peptide and the negatively charged membrane of the bacterium. The peptide S1-F2 was able to interact with negatively charged lipid (Figure 5), indicating that S1 binds in two steps: a fast electrostatic step and a second slower step mediated by the hydrophobic effect. However, S1-F2 on its own appeared insufficient to neutralize LPS or to display antimicrobial activity. In the case of MIRIAM, the MIR-F1 appears to be necessary for the strong binding while MIR-F2 is mechanistically important. In other words MIR-F1 drives the binding so that the C-terminal portion achieves sufficiently high concentrations on the membrane to exert its function. MIRIAM's hydrophobic motif seems to be different from the amphipathic helix found in the studied MIR-F1, which interacts with anionic lipids but again is not active in neutralizing LPS or killing GNB. Samples containing mixtures of both fragments (S1-F1 *and* S1-F2 or MIR-F1 *and* MIR-F2) displayed no cooperativity and lack biological activity. Therefore, it is reasonable to conclude that the length of the peptides and a close interaction of amino acids in a single molecule are crucial, potentially for an intramolecular interaction. Whether it is the length of the peptide which enables its spanning the membrane bilayer or the close proximity of differently functional entities within a peptide remains to be confirmed.

It is notable that S1 only causes minor hemolysis of about 13% at a concentration of 100 μg/mL, which is well beyond the microbicidal concentration. At the same concentration, MIRIAM caused 25% hemolysis, suggesting that rearrangement of the amino acid sequence increased the hemolytic activity albeit with a concomitant increase in the affinity for negatively charged lipids (Figure 2A). This effect on eukaryotic cells might also stem from the increased helicity of the peptide, which is known to correlate directly with cytotoxicity (*38*).

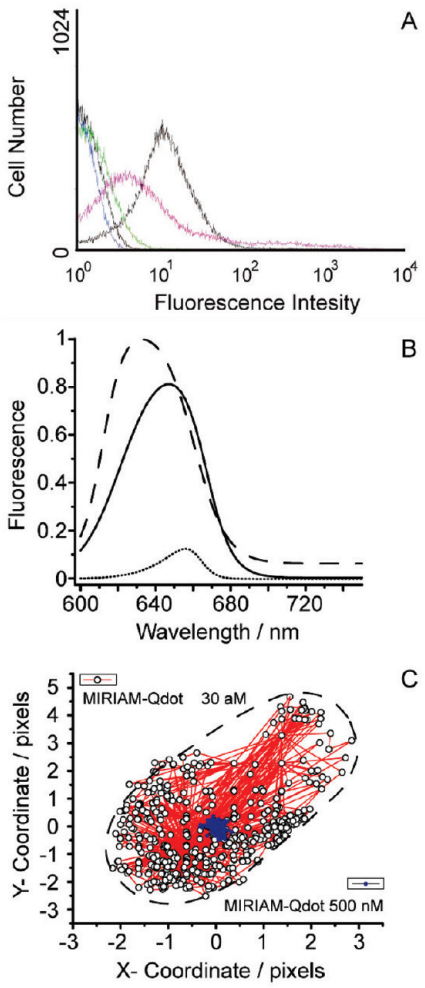

FIGURE 7: Qdot-labeled peptide characteristics and single particle tracking. (A) Fluorescence activated cell sorting of *E. coli* stained with various peptide-Qdot655 conjugates. Black, S1-Qdot; purple, MIRIAM-Qdot; green, negS1-Qdot; black, biotin-Qdot; blue, *E. coli* autofluorescence. (B) Fluorescence emission spectra of peptide-Qdot conjugates. As reported previously, the emission of S1-Qdot in the *E. coli* membrane shifts to lower wavelengths (*8*). In the case of MIRIAM-Qdot the shift is not as prominent but still significant compared to the minor binding of negS1-Qdot, where the emission corresponds to the emission of the free Qdot measured in aqueous or organic (tetrahydrofuran) solvents (data not shown). (C) Single particle tracking of MIRIAM-Qdot conjugate on live *E. coli* using TIRF microscopy. Representative image of trajectories of Qdot conjugate movement tracked over 1000 frames corresponding to 4000 ms. The lateral diffusion coefficient (D_{lat}) was calculated to be 5.52 $\mu m^2/s$.

In our previous study, we observed that S1 binds primarily to membranes of GNB and therefore is unlikely to interact with intracellular targets (*8*). While a minor percentage (7%) of S1 was found in the cytosol, MIRIAM conjugates were only found attached to membranes. This indicates that the dissociation of MIRIAM from the membrane is a rare event which is concordant with the results obtained using SPR. Furthermore, TEM micrographs showed that MIRIAM detaches the membranes from bacteria (Figure 6). Whether this is a specific effect of MIRIAM acting on GNB remains to be confirmed.

Our data obtained by TIRF microscopy SPT suggests that at active peptide concentrations an association event occurs in which peptides form clusters of high concentration in order to exert their function on the membrane, which is consistent with the mechanism of action of S1 (*8*). However, whether this process is solely a multimerization event or whether it is accompanied by an integration step remains to be confirmed. The observed deceleration in the mobility of MIRIAM is nevertheless likely to be caused by association even if it precedes integration since this process only happens at a certain peptide concentration threshold.

The results of our study show that both, the parental and the new peptide despite their obvious sequence dissimilarity, share the same basic mechanism of action with slight variations such as higher affinity for negatively charged lipids or higher content of α-helical structure. However, the fragments show that the moieties interacting with lipids are now in different positions of the peptides. On the basis of our data, we conclude that in order to create a fully functional AMP with the desired high therapeutic value (cell type selectivity and high antimicrobial activity), the combination of charge and hydrophobicity plays the most important role but only in a carefully balanced ensemble of sequence position and secondary structure. The observations using the full-length peptide might indicate that the length of the peptides is of significance too, either in order to span the lipid bilayer or may stem from the necessity of differently functional entities being in close proximity in order to contribute to the function of the peptide. Our findings show that a potential way of designing an AMP-based drug might be to structurally mimic naturally occurring peptides, using their molecular building blocks as templates to create new peptides.

ACKNOWLEDGMENT

The authors thank James R. Thompson (Harvard Medical School, USA) and Belinda Loh (University of Oxford, U.K.) for critically reading the manuscript.

SUPPORTING INFORMATION AVAILABLE

Structure change of full-length S1 in SDS and POPG/POPE measured by CD spectroscopy (Figure 1); IC_{50} value of MIRIAM on LPS-induced rFC activation (Figure 2); functional analysis of MIR-F1, MIR-F2 and S1-F1, S1-F2 peptides using the LPS neutralization assay (Figure 3); FACS on *E. coli* stained with AMP-Qdot655 conjugate (Figure 4); biological and biophysical characteristics of full-length peptides and fragments (Table 1). This material is available free of charge via the Internet at http://pubs.acs.org.

REFERENCES

1. Zasloff, M. (2002) Antimicrobial peptides of multicellular organisms. *Nature 415*, 389–395.
2. Wang, G., Li, X., and Wang, Z. (2009) APD2: the updated antimicrobial peptide database and its application in peptide design. *Nucleic Acids Res. 37*, 933–937.
3. Scott, M. G., and Hancock, R. E. (2000) Cationic antimicrobial peptides and their multifunctional role in the immune system. *Crit. Rev. Immunol. 20*, 407–431.
4. Brown, K. L., and Hancock, R. E. (2006) Cationic host defense (antimicrobial) peptides. *Curr. Opin. Immunol. 18*, 24–30.
5. Hancock, R. E. (2001) Cationic peptides: effectors in innate immunity and novel antimicrobials. *Lancet Infect. Dis. 1*, 156–164.
6. Davies, J. (1994) Inactivation of antibiotics and the dissemination of resistance genes. *Science 264*, 375–382.
7. Yeaman, M. R., and Yount, N. Y. (2003) Mechanisms of antimicrobial peptide action and resistance. *Pharmacol. Rev. 55*, 27–55.
8. Leptihn, S., Har, J. Y., Chen, J., Ho, B., Wohland, T., and Ding, J. L. (2009) Single molecule resolution of the antimicrobial action of quantum dot-labeled sushi peptide on live bacteria. *BMC Biol. 7*, 22.
9. Maloy, W. L., and Kari, U. P. (1995) Structure-activity studies on magainins and other host defense peptides. *Biopolymers 37*, 105–122.

10. Ding, J. L., Li, P., and Ho, B. (2008) The Sushi peptides: structural characterization and mode of action against Gram-negative bacteria. *Cell. Mol. Life Sci. 65*, 1202–1219.
11. Wieprecht, T., Dathe, M., Krause, E., Beyermann, M., Maloy, W. L., MacDonald, D. L., and Bienert, M. (1997) Modulation of membrane activity of amphipathic, antibacterial peptides by slight modifications of the hydrophobic moment. *FEBS Lett. 417*, 135–140.
12. Kim, S., Kim, S. S., and Lee, B. J. (2005) Correlation between the activities of alpha-helical antimicrobial peptides and hydrophobicities represented as RP HPLC retention times. *Peptides 26*, 2050–2056.
13. Okuda, D., Yomogida, S., Kuwahara-Arai, K., Hitamatsu, K., Tamura, H., and Nagaoka, I. (2009) Augmentation of the antimicrobial activities of guinea pig cathelicidin CAP11-derived peptides by amino acid substitutions. *Int. J. Mol. Med. 23*, 501–508.
14. Rosenfeld, Y., Sahl, H. G., and Shai, Y. (2008) Parameters involved in antimicrobial and endotoxin detoxification activities of antimicrobial peptides. *Biochemistry 47*, 6468–6478.
15. Chou, H. T., Kuo, T. Y., Chiang, J. C., Pei, M. J., Yang, W. T., Yu, H. C., Lin, S. B., and Chen, W. J. (2008) Design and synthesis of cationic antimicrobial peptides with improved activity and selectivity against Vibrio spp. *Int. J. Antimicrob. Agents 32*, 130–138.
16. Monincova, L., Budesinsky, M., Slaninova, J., Hovorka, O., Cvacka, J., Voburka, Z., Fucik, V., Borovickova, L., Bednarova, L., Straka, J., and Cerovsky, V. (2010) Novel antimicrobial peptides from the venom of the eusocial bee *Halictus sexcinctus* (Hymenoptera: Halictidae) and their analogs. *Amino Acids 39* (3), 763–775.
17. Takeshima, K., Chikushi, A., Lee, K. K., Yonehara, S.and Matsuzaki, K. (2003) Translocation of analogues of the antimicrobial peptides magainin and buforin across human cell membranes. *J. Biol. Chem. 278*, 1310–1315.
18. Pathak, N., Salas-Auvert, R., Ruche, G., Janna, M. H., McCarthy, D., and Harrison, R. G. (1995) Comparison of the effects of hydrophobicity, amphiphilicity, and alpha-helicity on the activities of antimicrobial peptides. *Proteins 22*, 182–186.
19. Rosenfeld, Y., Lev, N., and Shai, Y. (2010) Effect of the hydrophobicity to net positive charge ratio on antibacterial and anti-endotoxin activities of structurally similar antimicrobial peptides. *Biochemistry 49*, 853–861.
20. Dathe, M., and Wieprecht, T. (1999) Structural features of helical antimicrobial peptides: their potential to modulate activity on model membranes and biological cells. *Biochim. Biophys. Acta 1462*, 71–87.
21. Dathe, M., Wieprecht, T., Nikolenko, H., Handel, L., Maloy, W. L., MacDonald, D. L., Beyermann, M., and Bienert, M. (1997) Hydrophobicity, hydrophobic moment and angle subtended by charged residues modulate antibacterial and haemolytic activity of amphipathic helical peptides. *FEBS Lett. 403*, 208–212.
22. Wieprecht, T., Apostolov, O., Beyermann, M., and Seelig, J. (1999) Thermodynamics of the alpha-helix-coil transition of amphipathic peptides in a membrane environment: implications for the peptide-membrane binding equilibrium. *J. Mol. Biol. 294*, 785–794.
23. Wieprecht, T., Dathe, M., Beyermann, M., Krause, E., Maloy, W. L., MacDonald, D. L., and Bienert, M. (1997) Peptide hydrophobicity controls the activity and selectivity of magainin 2 amide in interaction with membranes. *Biochemistry 36*, 6124–6132.
24. Wieprecht, T., Dathe, M., Epand, R. M., Beyermann, M., Krause, E., Maloy, W. L., MacDonald, D. L., and Bienert, M. (1997) Influence of the angle subtended by the positively charged helix face on the membrane activity of amphipathic, antibacterial peptides. *Biochemistry 36*, 12869–12880.
25. Bechinger, B. (1999) The structure, dynamics and orientation of antimicrobial peptides in membranes by multidimensional solid-state NMR spectroscopy. *Biochim. Biophys. Acta 1462*, 157–183.
26. Matsuzaki, K., Murase, O., Fujii, N., and Miyajima, K. (1996) An antimicrobial peptide, magainin 2, induced rapid flip-flop of phospholipids coupled with pore formation and peptide translocation. *Biochemistry 35*, 11361–11368.
27. Shin, S. Y., Kang, J. H., and Hahm, K. S. (1999) Structure-antibacterial, antitumor and hemolytic activity relationships of cecropin A-magainin 2 and cecropin A-melittin hybrid peptides. *J. Pept. Res. 53*, 82–90.
28. Kloczkowski, A., Ting, K. L., Jernigan, R. L., and Garnier, J. (2002) Combining the GOR V algorithm with evolutionary information for protein secondary structure prediction from amino acid sequence. *Proteins 49*, 154–166.
29. Luo, P., and Baldwin, R. L. (1997) Mechanism of helix induction by trifluoroethanol: a framework for extrapolating the helix-forming properties of peptides from trifluoroethanol/water mixtures back to water. *Biochemistry 36*, 8413–8421.
30. Udenfried, S. (1969) Fluorescence Assay in Biology and Medicine, Academic Press, New York.
31. Jain, M. K., Rogers, J., Simpson, L., and Gierasch, L. M. (1985) Effect of tryptophan derivatives on the phase properties of bilayers. *Biochim. Biophys. Acta 816*, 153–162.
32. Chen, Y., and Barkley, M. D. (1998) Toward understanding tryptophan fluorescence in proteins. *Biochemistry 37*, 9976–9982.
33. Hasselbacher, C. A., Rusinova, E., Waxman, E., Rusinova, R., Kohanski, R. A., Lam, W., Du Guha, A. J., Lin, T. C., and Polikarpov, I. (1995) Environments of the four tryptophans in the extracellular domain of human tissue factor: comparison of results from absorption and fluorescence difference spectra of tryptophan replacement mutants with the crystal structure of the wild-type protein. *Biophys. J. 69*, 20–29.
34. Magde, D., Elson, E. L., and Webb, W. W. (1972) Thermodynamic fluctuations in a reacting system: measurement by fluorescence correlation spectroscopy. *Phys. Rev. Lett.* 705–708.
35. Bessalle, R., Haas, H., Goria, A., Shalit, I., and Fridkin, M. (1992) Augmentation of the antibacterial activity of magainin by positive-charge chain extension. *Antimicrob. Agents Chemother. 36*, 313–317.
36. Schumann, M., Dathe, M., Wieprecht, T., Beyermann, M., and Bienert, M. (1997) The tendency of magainin to associate upon binding to phospholipid bilayers. *Biochemistry 36*, 4345–4351.
37. Brogden, K. A. (2005) Antimicrobial peptides: pore formers or metabolic inhibitors in bacteria? *Nat. Rev. Microbiol. 3*, 238–250.
38. Giangaspero, A., Sandri, L., and Tossi, A. (2001) Amphipathic alpha helical antimicrobial peptides. *Eur. J. Biochem./FEBS 268*, 5589–5600.